Journal of Electroceramics 5:2, 81–92, 2000

Percolation in Composites

ARMIN BUNDE
Institut für Theoretische Physik III, Justus-Liebig-Universität Giessen, Heinrich-Buff-Ring 16, D-35392 Giessen, Germany
bunde@physik.uni-giessen.de

WOLFGANG DIETERICH
Universität Konstanz, Fakultät für Physik, Univesitätsstraße 10, D-78457 Konstanz,
wolfgang.dieterich@uni-konstanz.de

Submitted September 15, 1999, Revised November 30, 1999; Accepted November 30, 1999

Abstract. Many properties of composite materials such as diffusion, electrical conduction, dielectric response as well as elasticity, are intimately related to the geometrical arrangement of the constitutive phases, including the geometry of the respective interfaces. Percolation theory, whose objective is to characterize the connectivity properties in random geometries and to explore them with respect to physical processes, thus provides a natural frame for the theoretical description of random composites. This article explains basic concepts of static percolation theory and percolative transport, which subsequently are applied to specific experiments on heterogeneous ionic conductors.

Keywords: percolation, random resistor network, critical exponent, universality, composite ionic conductors, nanocrystalline ionic conductors

1. Introduction

Percolation is a standard model for disordered systems, with widespread applications in nature. Here we focus on percolation models for composites. It is essential to note that because of universality the results following from percolation theory do not depend on certain irrelevant details of the specific model used, and general scaling laws can be deduced.

In the first part of this review we give a brief introduction into static aspects of the standard percolation theory. In the second part, we describe quite generally diffusion and electrical conduction in percolation systems. In the third part, finally, we demonstrate the utility of percolation concepts in understanding electrical transport in composite ionic conductors, where interfacial conduction plays a predominant role.

2. Lattice and Continuum Percolation

2.1. The Models

Percolation represents the basic model for a structurally disordered system (for recent reviews see [1–3]). For simplicity, let us consider a square lattice, where each site is occupied randomly with probability p or is empty with probability $1 - p$ (see Fig. 1). Occupied and empty sites may stand for very different physical properties. For illustration, let us assume that the occupied sites are electrical conductors, the empty sites represent insulators, and that electrical current can only flow between nearest-neighbor conductor sites. Two-phase heterogeneous mixtures like AgCl/α-AgI may be viewed as (three-dimensional) percolation systems, where the occupied sites represent AgI and the empty sites AgCl [4].

At low concentration p, the conductor sites are either isolated or form small clusters of nearest-neighbor sites. Two conductor sites belong to the same cluster if they are connected by a path of nearest-neighbor conductor sites, and a current can flow between them. At low p values, the mixture is an insulator, since no conducting path connecting opposite edges of our lattice exists. At large p values on the other hand many conducting paths between opposite edges exist, where electrical current can flow, and the mixture is a conductor. At some concentration in between, therefore, a threshold

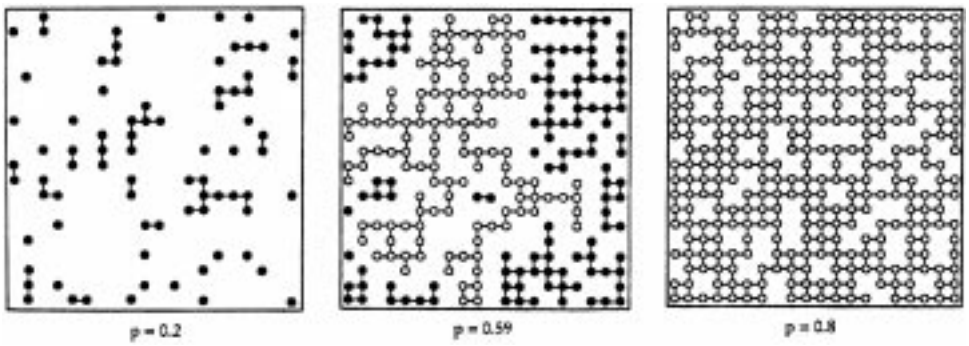

Fig. 1. Site percolation on the square lattice: The small circles represent the occupied sites for three different concentrations: $p = 0.2$, 0.59, and 0.80. Nearest-neighbor cluster sites are connected by lines representing the bonds. Filled circles are used for finite clusters, while open circles mark the large *infinite* cluster.

concentration p_c must exist where for the first time electrical current can *percolate* from one edge to the other. Below p_c we have an insulator, above p_c we have a conductor. The threshold concentration is called the *percolation threshold*, or, since it separates two different phases, the *critical concentration*.

A nice example of such a percolation system is irradiated polyimide, where KrF excimer laser pulses of an intensity greater than $20\,\text{mJ/cm}^2$ induce a conductivity change in a thin surface layer on the polymer. The interaction of the intense laser pulse with the polymer decomposes portions of a thin surface layer into small carbon clusters of about 50 nm diameter. These carbon clusters are electrically conducting and represent the occupied sites. The density of the carbon cluster can be increased by successive laser shots. At the percolation threshold, one observes conduction over macroscopic areas [5].

If the occupied sites are superconductors and the empty sites are conductors, p_c separates a normal-conducting phase (below p_c) from a superconducting phase (above p_c). A quite different example is a mixture of ferromagnets and paramagnets, where the system changes at p_c from paramagnetic to ferromagnetic.

In contrast to the more common thermal phase transitions, where the transition between two phases occurs at a critical temperature, the *percolation transition* described here is a *geometrical phase transition*, which is characterized by the geometric features of large clusters in the neighborhood of p_c. At low values of p only small clusters of occupied sites exist. When the concentration p is increased the average size of the clusters increases. At the critical concentration p_c a large cluster appears which connects opposite edges of the lattice. We call this cluster the *infinite* cluster, since its size diverges in the thermodynamic limit. When p is increased further the density of the infinite cluster increases, since more and more sites become part of the infinite cluster, and the average size of the *finite* clusters, which do not belong to the infinite cluster, decreases. At $p = 1$, trivially, all sites belong to the infinite cluster.

The critical concentration depends on the details of the lattice and increases, for fixed dimension d, with decreasing coordination number z of the lattice: For the triangular lattice, $z = 6$ and $p_c = 1/2$, for the square lattice, $z = 4$ and $p_c \cong 0.592746$, and for the honeycomb lattice, $z = 3$ and $p_c \cong 0.6962$. For fixed z, p_c decreases if the dimension d is enhanced. In both the triangular lattice and the simple cubic lattice we have $z = 6$, but p_c for the simple cubic lattice is considerably smaller, $p_c \cong 0.3116$.

So far we have considered *site percolation*, where the sites of a lattice have been occupied randomly. When the sites are all occupied, but the bonds between the sites are randomly occupied with probability q, we speak of *bond percolation* (see Fig. 2a). Two occupied bonds belong to the same cluster if they are connected by a path of occupied bonds, and the critical concentration q_c of bonds ($q_c = 1/2$ in the square lattice and $q_c \simeq 0.2488$ in the simple cubic lattice) separates a phase of finite clusters of bonds from a phase with an infinite cluster.

If sites are occupied with probability p *and* bonds are occupied with probability q, we speak of *site–bond percolation*. Two occupied sites belong to the same cluster if they are connected by a path of nearest-neighbor occupied sites with occupied bonds in between. For $q = 1$, site-bond percolation reduces to site percolation, for $p = 1$ it reduces to bond

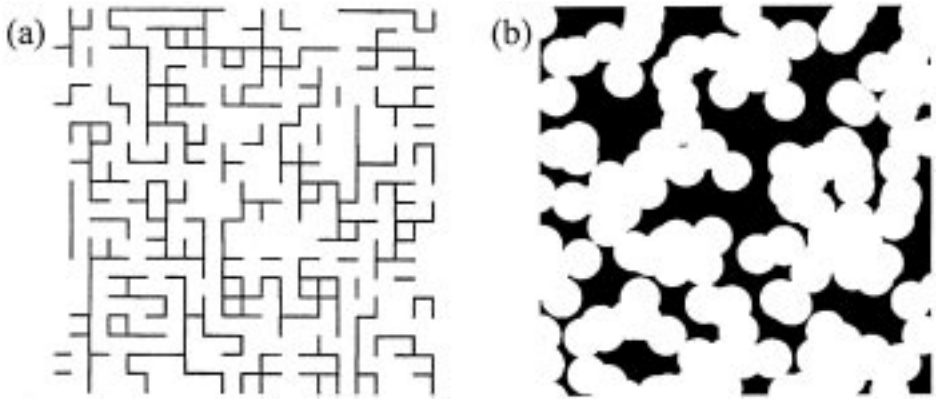

Fig. 2. Further percolation systems: (a) Bond percolation cluster on a square lattice and (b) continuum percolation of circular discs with fixed radius at the percolation threshold.

percolation. In general, both parameters characterize the state of the system. Accordingly, a *critical line* in (p, q) space separates both phases, which for $p = 1$ and $q = 1$ takes the values of the critical bond and site concentrations, respectively.

Perhaps the most common example of bond percolation in physics is a *random resistor network*, where the metallic wires in a regular network are cut randomly with probability $1 - q$. Here q_c separates a conductive phase at large q from an insulating phase at low q. A possible application of bond percolation in chemistry is the polymerization process, where small branching molecules can form large molecules by activating more and more bonds between them. If the activation probability q is above the critical concentration, a network of chemical bonds spanning the whole system can be formed, while below q_c only macromolecules of finite size can be generated. This process is called a *sol-gel* transition. An example of this *gelation* process is the boiling of an egg, which at room temperature is liquid and upon heating becomes a more solid-like *gel*. Site-bond percolation can be relevant for gelation in dilute media.

The most natural example of percolation is *continuum percolation*, where the positions of the two components of a random mixture are not restricted to the discrete sites of a regular lattice. As a simple example, consider a sheet of conductive material, with circular holes punched randomly in it (see Fig. 2b). The relevant quantity now is the fraction p of remaining conductive material. Compared with site and bond percolation, the critical concentration is further decreased: $p_c \cong 0.312$ for $d = 2$, when all circles have the same radius. This picture can easily be generalized to three dimensions, where spherical voids are generated randomly in a cube, and $p_c \cong 0.034$. Due to its similarity to Swiss cheese, this model of continuous percolation is called the Swiss cheese model. Similar models, where also the size of the spheres can vary, are used to describe sandstone and other porous materials.

In all cases, the percolation transition is characterized by the geometrical properties of the clusters in the critical regime $|p - p_c|/p_c \ll 1$ near p_c. The probability P_∞ that a site belongs to the infinite cluster is zero below p_c and increases above p_c (in the critical regime) as

$$P_\infty \sim (p - p_c)^\beta \tag{1}$$

This behavior is illustrated in Fig. 3. The linear size of the *finite* clusters, below and above p_c, is characterized by the *correlation length* ξ. The correlation length is defined as the mean distance between two sites on the same finite cluster and represents the characteristic length scale in percolation. When p approaches p_c, ξ increases as

$$\xi \sim |p - p_c|^{-\nu} \tag{2}$$

with the same exponent ν below and above the threshold (see also Fig. 3).

Very important is the universal behavior of these static exponents: While p_c depends explicitly on the type of percolation system considered, the *critical exponents* β and ν are universal and depend neither on the structural details of the lattice (e.g., square or triangular) nor on the type of percolation (site, bond, or continuum), but only on the dimension d of the

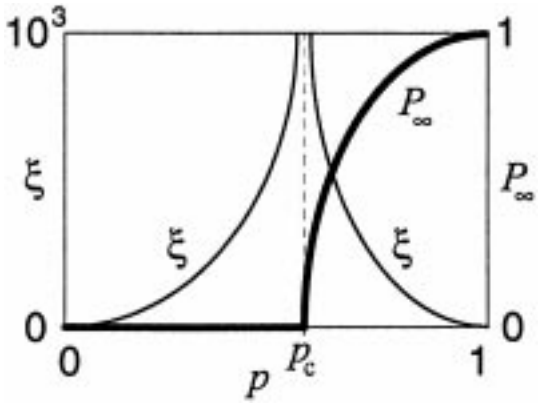

Fig. 3. Schematic diagram of the probability P_∞ (bold line, see Eq. (1)) and the correlation length ξ (thin line, see Eq. (2)) versus the concentration p of occupied sites.

lattice. The values of the critical exponents are given in Table 1 for two and three dimensions.

2.2. *The Fractal Structure of Percolation Clusters near p_c*

Near p_c on length scales smaller than ξ both the infinite cluster and the finite clusters are self-similar, i.e., if we cut a small part out of a large cluster, magnify it to the original cluster size and compare it with the original, we cannot tell the difference: Both look the same. On length scales well above ξ, the infinite percolation cluster is a compact structure, but below ξ the cluster is a fractal and self-similar. This feature is illustrated in Fig. 4, where the infinite percolation cluster above p_c is shown in four different magnifications. When the scale is sufficiently small (as in the two figures on the bottom), the cluster is selfsimilar and original and further magnifications do not change the essential picture.

For comparison, Fig. 5 shows a real percolation cluster close to the critical concentration, made of a thin gold film evaporated on amorphous Si_3N_4. Both the artificial cluster at small length scales and the natural cluster look quite the same.

As a consequence of the (non-trivial) self-similarity on length scales below ξ, the cluster is characterized by a ''fractal'' dimension: The mean mass of the cluster within a circle of radius r increases with r as $M(r) \sim r^{d_f}$ with the ''fractal dimension'' d_f. The numerical values of d_f can be found in Table 1. Above p_c on length scales *larger* than ξ the infinite cluster can be regarded as a homogeneous system which is composed of many cells of size ξ. Mathematically, this can be summarized as

$$M(r) \sim \begin{cases} r^{d_f} & \text{if } r \ll \xi \\ r^{d} & \text{if } r \gg \xi \end{cases} \tag{3}$$

The fractal dimension d_f can be related to β and ν in the following way: Above p_c, the mass M_∞ of the infinite cluster in a large lattice of size L^d is proportional to $L^d P_\infty$. On the other hand, this mass is also proportional to the number of unit cells of size ξ, $(L/\xi)^d$, multiplied by the mass of each cell which is proportional to ξ^{d_f}. This yields (with Eqs. (1) and (2))

$$\begin{aligned} M_\infty &\sim L^d P_\infty \sim L^d (p - p_c)^\beta \sim (L/\xi)^d \xi^{d_f} \\ &\sim L^d (p - p_c)^{\nu d - \nu d_f} \end{aligned} \tag{4}$$

and hence, comparing the exponents of $(p - p_c)$,

$$d_f = d - \frac{\beta}{\nu} \tag{5}$$

Since β and ν are universal exponents, d_f is also universal.

3. Diffusion and Conductivity

3.1. *Equivalence Between Diffusion and Conduction*

Electrical conduction is one of the most common probes in the investigation of composites. To

Table 1. Critical exponents and fractal dimensions for percolation in two and three dimensions. The numerical values are taken from [1]. (As is always the case in critical phenomena, the power–law dependencies only hold in the critical regime, see also Table 2.)

Quantity		Exponent	$d = 2$	$d = 3$
Order parameter	$P_\infty(p) \sim (p - p_c)^\beta$	β	5/36	0.417 ± 0.003
Correlation length	$\xi(p) \sim \lvert p - p_c \rvert^{-\nu}$	ν	4/3	0.875 ± 0.008
Cluster mass	$M(r) \sim r^{d_f}$	d_f	91/48	2.524 ± 0.008

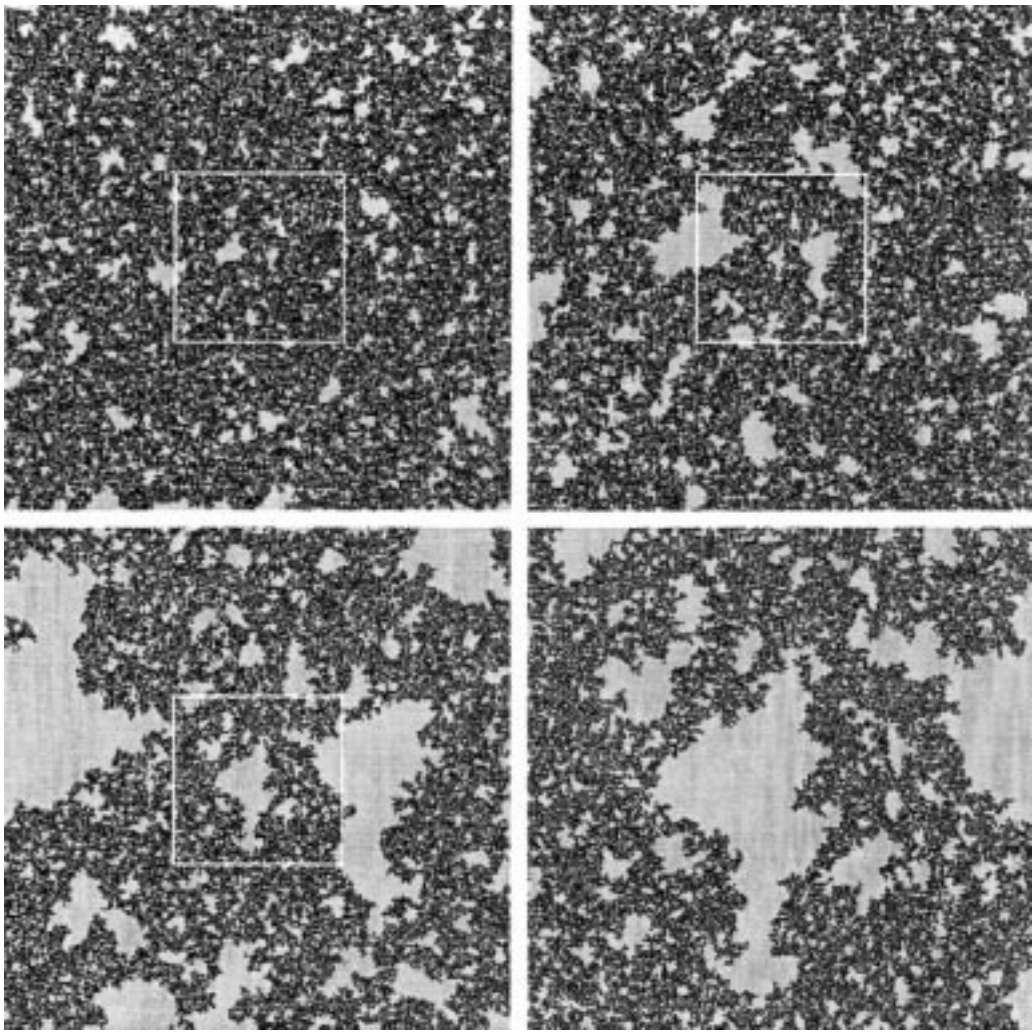

Fig. 4. Self-similarity of the infinite percolation cluster on the square lattice above the critical concentration ($p = 0.595$). In the upper left figure, the length of the system is larger than the correlation length, and therefore the cluster looks compact. The linear size of the two bottom figures is smaller than the correlation length, exhibiting the self-similar structure of the cluster at sufficiently small length scales (courtesy of J. Kantelhardt).

interprete such measurements it is therefore necessary to develop theoretical tools for calculating the macroscopic (averaged) conductivity σ of a heterogeneous material. An efficient procedure is to exploit the well-known equivalence between conduction and diffusion problems.

In the special case of a dilute system of charged defects, the conductivity σ and the defect diffusion constant D are related by the Nernst-Einstein relation, see Eq. (7). Moreover, irrespective of microscopic details of the conduction mechanism, an exact equivalence between an electrostatic problem and a corresponding stationary diffusion problem can be established on purely macroscopic grounds. Let $\sigma(\vec{r})$ denote the local conductivity in a heterogeneous material and $D(\vec{r})$ the local diffusion constant in the diffusion problem, where $D(\vec{r})$ has the same spatial dependence as $\sigma(\vec{r})$. Obviously, Ohm's law for the electrical current density, $\vec{j}_{el}(\vec{r}) = -\sigma(\vec{r})\vec{\nabla}\varphi(\vec{r})$ and Fick's law for the diffusion current density, $\vec{j}_D = -D(\vec{r})\vec{\nabla}p(\vec{r})$ are formally identical. Here $\varphi(\vec{r})$ and $p(\vec{r})$ denote the electrostatic potential and

Fig. 5. Gold film evaporated on amorphous Si_3N_4 (after [6]).

the density of diffusing particles, respectively. Under stationary conditions, both currents have zero divergence within the medium. Hence the two problems of calculating the total conductivity σ and the total diffusion constant D are mathematically equivalent. Often, calculation of D through random walk theories and stochastic simulation is more efficient than directly solving the electrostatic equations. In the next two subsections we shall therefore concentrate on concepts of diffusion in ordered and disordered media, which in most cases are represented in the form of discrete networks.

3.2. Transport in Regular Lattices

After we have discussed the structural properties of percolation systems close to the percolation threshold, see section 2, we will now focus on the *dynamical* properties of percolation systems, where to each site or bond a physical property such as conductivity is assigned. We show that due to the fractal nature of the percolation clusters near p_c, the physical laws of dynamics are changed essentially and become *anomalous*.

At first, we consider regular lattices. The diffusion process is commonly modeled by a simple random walk, which advances one step of length ℓ in one time unit τ. Each step brings the random walker to a randomly chosen nearest-neighbor site on a given d-dimensional lattice. Assuming that jumps at different steps are uncorrelated, we obtain $\langle r^2(t)\rangle = \ell^2 t/\tau$, which is equivalent to Fick's first law. In the general case, when the lengths ℓ of the steps of the random walker as well as the time τ between successive steps may vary, this relation is modified into

$$\langle r^2(t)\rangle = 2dDt \tag{6}$$

where $D = \langle \ell^2\rangle/\langle\tau\rangle$ is the *diffusion coefficient*. The brackets are averages over many steps and configurations. The diffusion coefficient is related to the dc-conductivity $\sigma_{\rm dc}$ by the Nernst-Einstein equation,

$$\sigma_{\rm dc} = n(e^2/k_BT)D \tag{7}$$

where n is the density and e the charge of the diffusing particles. Next we consider disordered structures.

3.3. Percolation Clusters

We start with the infinite percolation cluster at the critical concentration p_c. The cluster has loops and dangling ends, and both substructures slow down the motion of a random walker. Due to self-similarity, loops and dangling ends occur on all length scales, and therefore the motion of the random walker is slowed down on *all* length scales. The time t the walker needs to travel a distance R is no longer, as in regular systems, proportional to R^2, but scales as $t \sim R^{d_w}$, where $d_w > 2$ is the *fractal dimension of the random walk* [1,2]. For the mean-square displacement this yields immediately

$$\langle r^2(t)\rangle \sim t^{2/d_w} \tag{8}$$

The fractal dimension d_w is approximately equal to $3d_f/2$ [7]; the results of numerical simulations can be found in Table 1. For continuum percolation (Swiss cheese model) in $d = 3$, d_w is enhanced: $d_w \cong 4.2$ [8]. Diffusion processes described by Eq. (8) are generally referred to as *anomalous diffusion*.

Above p_c, fractal structures occur only within the correlation length $\xi(p)$ given by Eq. (2). Thus the anomalous diffusion law, Eq. (8), occurs only below the corresponding crossover time $t_\xi \sim R(t_\xi)^{d_w} \sim \xi^{d_w}$, which decreases proportional to $(p - p_c)^{-\nu d_w}$, if p is further increased. Above t_ξ, on large time scales, the random walker explores large length scales where the cluster is homogeneous, and $\langle r^2(t)\rangle$ follows Fick's law (Eq.(6)), increasing linearly with time t. Thus,

$$\langle r^2(t)\rangle \sim \begin{cases} t^{2/d_w} & \text{if } t \ll t_\xi \\ t & \text{if } t \gg t_\xi \end{cases} \tag{9}$$

The diffusion coefficient is related to the dc-conductivity $\sigma_{\rm dc}$ by the Nernst-Einstein equation, Eq. (7). Below p_c, there is no current between opposite edges of the system, and $\sigma_{\rm dc} = 0$. Above p_c, σ_{dc} increases by a power law (see Fig. 6 for illustration),

$$\sigma_{\rm dc} \sim (p - p_c)^{\mu} \tag{10}$$

where the critical exponent μ is (semi)-universal. For percolation on a lattice, μ depends only on d; the numerical results are contained in Table 2. For continuum percolation (Swiss cheese model) in $d = 3$, however, μ is enhanced: $\mu \cong 2.38$.

Combining Eqs. (7) and (10), we can obtain the behavior of the diffusion coefficient D as a function of $p - p_c$. Since only the particles on the infinite cluster contribute to the dc conductivity, we have (from Eq. (1)) $n \sim P_\infty \sim (p - p_c)^{\beta}$ in Eq. (7). This yields

$$D \sim (p - p_c)^{\mu - \beta} \tag{11}$$

Next we use scaling arguments (see, e.g., [1,2]) to relate the exponent μ to d_w. Equations (11) and (6) imply that above t_ξ, the mean-square displacement $\langle r^2(t)\rangle$ behaves as

$$\langle r^2(t)\rangle \sim (p - p_c)^{\mu-\beta} t, \quad t > t_\xi \tag{12}$$

On the other hand we know that for times below t_ξ on distances $r < t_\xi^{1/d_w}$,

$$\langle r^2(t)\rangle \sim t^{2/d_w}, \quad t < t_\xi \tag{13}$$

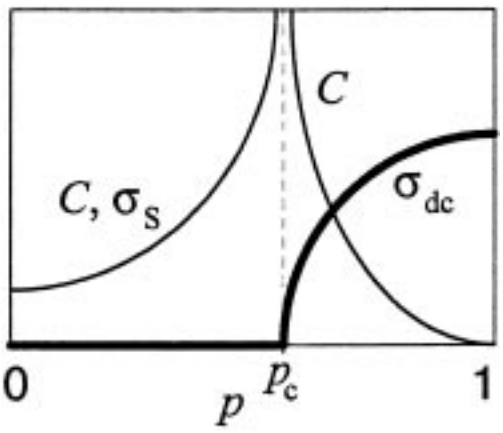

Fig. 6. Schematic diagram of the (usual) dc–conductivity σ_{dc} (bold line, see Eq. (10)) and the conductivity σ_S for a conductor-superconductor percolation network (see section 3.4, thin line for $p < p_c$) versus the concentration p of occupied sites. The cluster capacitance C is proportional to σ_s for $p < p_c$ and diverges with the same exponent for $p > p_c$ (see Eq. (17)).

By definition, for $t = t_\xi$, we have $\langle r^2(t)\rangle \sim \xi^2$. Substituting this into Eqs. (12) and (13) and equating both relations we obtain immediately $(p - p_c)^{\mu-\beta}$ $t_\xi \sim t_\xi^{2/d_w}$. Using $t_\xi \sim \xi^{d_w} \sim (p - p_c)^{-\nu d_w}$ (from Eq. (2)) we get the relation between μ and d_w,

$$d_w = 2 + (\mu - \beta)/\nu \tag{14}$$

3.4. Resistor–Capacitor Networks and ac-Conductivity

The random walk problems or the equivalent random resistor networks discussed in the foregoing subsection are now generalized to the case of an arbitrary two-component (AB) network, which can serve as an equivalent circuit model for the electrical properties at non-zero frequencies of arbitrary two-phase composites. Let us assume that each bond in the network represents (with probability p) a resistor with resistance $1/\sigma_A^0$ in parallel with a capacitor with capacitance C_A, or (with probability $1 - p$) a resistor with resistance $1/\sigma_B^0$ in parallel with a capacitor with capacitance C_B. The (complex) conductance of each bond is therefore either $\sigma_A = \sigma_A^0 + i\omega C_A$ or $\sigma_B = \sigma_B^0 + i\omega C_B$. At the percolation threshold, $p = p_c$, the total conductance in the case $|\sigma_A| \gg |\sigma_B|$ follows a power-law [1,9,10]

$$\sigma(\omega) \sim \sigma_A (\sigma_A/\sigma_B)^{-u} \tag{15}$$

where the exponent u has values $u = 0.5$ in $d = 2$ and $u \simeq 0.71$ in $d = 3$.

For extending this result to the critical regime below and above p_c, we multiply Eq. (15) by a complex scaling function $S_\pm(z)$ that depends on $z = |p - p_c|(\sigma_A/\sigma_B)^{\Phi}$. The two signs refer to the two different cases above and below p_c. Thus, for $|p - p_c|/p_c \ll 1$, we write [11,12]

$$\sigma(\omega) = \sigma_A (\sigma_A/\sigma_B)^{-u} \cdot S_\pm[|p - p_c|(\sigma_A/\sigma_B)^{\Phi}] \tag{16}$$

where, on account of Eq. (15), both S_+ and S_- become a constant as $|z| \to 0$. The exponent Φ as well as the asymptotic behavior of the scaling functions is determined by the asymptotic behavior of $\sigma(\omega)$ in the limit $\omega \to 0$ and $|\sigma_A/\sigma_B| \to \infty$.

Let us concentrate first on the resistor–capacitor (R–C) limit, where $\sigma_A = \sigma_A^0$ and $\sigma_B = i\omega C_B$, which pertains to random mixtures of a conductor and a dielectric. Below p_c, we have an insulator so that $\sigma(\omega)$

Table 2. Dynamical exponents for percolation in two and three dimensional lattices. The numerical values are taken from [1]

Quantity		Exponent	$d=2$	$d=3$
Random Walk	$\langle r^2(t)\rangle \sim t^{2/d_w}$	d_w	2.871 ± 0.001	3.80 ± 0.02
Conductivity	$\sigma_{\rm dc}(p) \sim (p-p_c)^{\mu}$	μ	1.30 ± 0.002	1.99 ± 0.01
Superconductivity	$\sigma_S(p) \sim (p-p_c)^{-s}$	s	1.30 ± 0.002	0.74 ± 0.03

must behave as $\sigma(\omega) \simeq i\omega C$ for $\omega \to 0$, with C the capacitance of the whole system. To satisfy this condition we must require $S_-(z) \simeq z^{-s}$ for $|z| \gg 1$, with $s = (1-u)/\Phi$. It follows that [11]

$$C \sim |p-p_c|^{-s} \tag{17}$$

On approaching the percolation threshold, the total capacitance therefore diverges according to the critical exponent s. This divergence of C has a simple physical interpretation: each pair of neighbored clusters forms a capacitor. The effective surface increases when p_c is approached and tends to infinity at p_c. Accordingly, the effective capacitance C of the system also diverges. Taking the limit $|\sigma_A| \to \infty$ in Eq. (16) it is easily seen that the same exponent s describes the divergence of the total conductivity near p_c in a normal conductor–superconductor network (cf. also Fig. 6).

On the other hand, Eq. (16) for $p > p_c$ must be consistent with $\sigma_{\rm dc} \sim (p-p_c)^{\mu}$, (see section 3.3), requiring that $S_+(z) \simeq z^{\mu}$ for $|z| \gg 1$ and $u = \Phi\mu$. Combining the above relations for the scaling exponent Φ, we can reexpress u and Φ in terms of s and μ, which yields

$$u = \frac{\mu}{\mu+s} \quad ; \quad \Phi = \frac{1}{\mu+s} \tag{18}$$

Next, we study a random mixture of a good conductor (A) and a ''leaky dielectric'' (B), where $\sigma_A^0/\sigma_B^0 = \tau \gg 1$. From Eq. (16) it is clear that for $|p-p_c|\tau^{\Phi} \ll 1$ the ac-conductivity is given by

$$\sigma(\omega) \sim \sigma_A \tau^{-u}(1 + i\omega C_B/\sigma_B^0)^u \tag{19}$$

Keeping τ fixed and approaching p_c, the total capacitance therefore exhibits a peak with a maximum

$$C \sim \tau^{1-u} \tag{20}$$

at the percolation threshold.

To describe the ac-response of conductor–dielectric mixtures at higher frequencies, inductive elements can be included in the model. RLC-networks have in fact been studied in connection with the optical response of metal–dielectric composites [13].

3.5. *Computational Methods*

In section (3.1) we have seen that the zero-frequency conductivity $\sigma_{\rm dc}$ of a heterogeneous mixture can be obtained via the random walk methodology. In fact, most studies in the literature concerning percolative transport in random mixtures, including critical exponents for percolation and the associated scaling properties, habe been obtained from simulations of the time-dependent mean-square displacement of a random walker. Monte Carlo and exact enumeration techniques are most common in that respect [14]. Ac-properties of mixtures, modeled for example by apropriate resistor–capacitor networks, can be calculated efficiently by the transfer-matrix method. For details we refer to the original work of Derrida and Vannimenus [15].

In many cases one is interested predominantly in the overall behavior of a mixture rather than in its detailed critical properties near a percolation threshold. Various forms of effective medium theory (EMT) [16] are useful in that respect. Concerning disorder and the percolation transition, the EMT plays a role analogous to mean-field theory in the context of thermal phase transitions. The simplest case is the single-bond EMT for bond-disordered networks. Let us assume a d-dimensional simple cubic multi-component network, where with probability p_α a bond has conductance σ_α. According to the EMT, the effective conductance of bonds, σ^{eff}, then is derived from the equation

$$\sum_\alpha p_\alpha \frac{\sigma^{eff} - \sigma_\alpha}{(z/2-1)\sigma^{eff} + \sigma_\alpha} = 0 \tag{21}$$

where $z = 2d$ is the coordination number of the network. Generally, near a percolation transition, the EMT yields mean-field critical exponents $\mu = s = 1$, independent of d. Extensions of the EMT to topologically disordered networks [17], continuous

media containing spherical or ellipsoidal inclusions [18–20] and random walks in the presence of energetic disorder [21,22] have also been studied extensively in the literature.

A more accurate way for obtaining dc- and ac-properties of bond-disordered networks is to use the real-space renormalization group approximation (RNG) [23,24]. The idea of this approach is to map the original network onto a coarse-grained, renormalized network where fluctuations in the local conductances on small scales have been averaged over. Iterating this procedure, one ends up with an ordered lattice, unless the iteration is started at a critical point, to be identified as a fixed point of that mapping. The RNG can well account for the overall conductance properties of the network and, in contrast to the EMT, yields non-trivial static and dynamic critical exponents. In $d = 2$ exact bond-transformations are known such that a finite network can be replaced by one effective bond [25].

4. Heterogeneous Ionic Conductors

4.1. Interfacial Percolation and the Liang-Effect

Let us now turn to percolation models that describe electrical transport in specific composite materials. A substantial amount of research has concentrated on ''dispersed ionic conductors'' after the discovery by Liang [26] that insulating fine particles with sizes of the order of 1 μm, dispersed in a conductive medium (e.g., Al_2O_3 in LiI), can lead to a conductivity enhancement [27]. This effect has been found to arise from the formation of a defective, highly conducting layer following the boundaries between the conducting and the insulating phase [28]. Effectively, the system thus contains three phases. Theoretical studies therefore have focused on suitable three-component impedance network models.

Figure 7 shows a two-dimensional illustration of such composites and a corresponding discretized model [29,30]. In its simplest version this model is constructed by randomly selecting a fraction p of elementary squares on a square lattice, which represent the insulating phase (C), while the remaining squares are the conducting phase (B). The distribution of both phases leads to a correlated bond percolation model with three types of bonds and associated bond conductances σ_α; $\alpha = A, B, C$; as defined in Fig. 7. For example, bonds in the boundary between phases B and C correspond to the highly conducting component (A). The analogous construction for three dimensions is obvious. Finite-frequency effects are readily included, when we allow bond conductances to be complex [31]. For simplicity, we may assume the ideal behavior $\sigma_\alpha = \sigma_\alpha^0 + i\omega C_\alpha$, including constant zero-frequency conductances σ_α^0 and capacitance elements C_α, but more general forms can be chosen when necessary. Clearly, the experimental situation described above requires that $\sigma_A^0/\sigma_B^0 = \tau \gg 1$; $\sigma_C^0 = 0$. Thereby it is natural to assume that σ_A^0 and σ_B^0 are thermally activated, such that their ratio $\tau \propto \exp(-\Delta E/k_B T)$ increases with decreasing temperature.

A remarkable feature of this model is the existence of two threshold concentrations. At $p = p_c'$, interface percolation (i.e., percolation of A-bonds) sets in, whereas at $p = p_c'' = 1 - p_c'$ (normally not accessible by experiment) the system undergoes a conductor-insulator transition. In two dimensions $(d = 2)$ we have $p_c' = 0.41$, while in $d = 3$, $p_c' = 0.097$, corre-

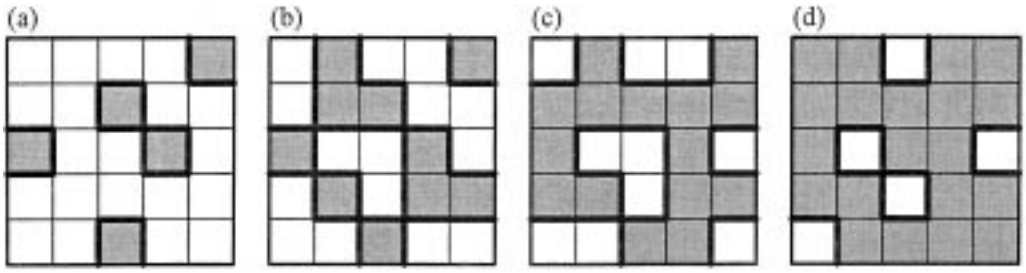

Fig. 7. Illustration of a three-component percolation model for dispersed ionic conductors, for different concentrations p of the insulating material. The insulator is represented by the gray area, the ionic conductor by the white area. The bonds can be highly conducting (A-bonds, bold lines), normal conducting (B-bonds), or insulating (C-bonds). (a) $p < p_c'$, (b) $p = p_c'$, (c) $p = p_c''$, (d) $p > p_c''$ (redrawn after [30]).

sponding to the threshold for second-neighbor $(d = 2)$ and third-neighbor $(d = 3)$ site percolation on a d-dimensional cubic lattice, respectively. At zero frequency, the total conductivity can be obtained from Monte Carlo simulation [29,30].

Figure 8 shows results for $d = 3$ and three different temperatures (corresponding to $\tau = 10, 30$ and 100). Good agreement with the experimental curves [32] is achieved, which show a broad maximum in the conductivity as a function of p in the range between the two thresholds. Changing τ (by varying the temperature) offers the possibility to interpret the measured activation energies as a function of p [33] and, in principle, also to detect the critical transport behavior associated with interface percolation. In the vicinity of p_c' it seems interesting in addition to study critical ac-effects. For example, at p_c' the effective capacitance develops a peak, whose height should scale with τ as $C_{eff} \sim \tau^{1-u}$, where $u = \mu/(\mu + s)$, see subsection 3.4. Ac-properties in the whole range of p-values have been calculated by renormalization group techniques (see subsection 3.5) [31].

Several extensions of this model are conceivable. In the case of dc-transport $(\omega = 0)$, the variation of the total conductivity with the size of dispersed particles has been calculated and successfully compared with experiments [34,35,37]. In particular, it was found that as the particle size decreases while the thickness of the highly conducting interfacial layer is fixed, the maximum in the total conductivity as a function of the insulator concentration p shifts to smaller values of p. The observation of conductivity maxima at very low volume fractions ($\simeq 10\%$) in certain composite electrolytes, however, was interpreted recently by a grain boundary mechanism within the bulk of the electrolyte phase [36].

Related work also emphasized aspects of continuum percolation in dispersed ionic conductors [35], which, depending on the geometrical conditions, can lead to dynamical critical properties differing from lattice percolation (see subsection 3.3).

4.2. Composite Micro- and Nanocrystalline Conductors

In the foregoing section, we have discussed dispersed ionic conductors that were prepared by melting the ionic conductor and adding the insulator (mainly Al_2O_3) to it. Next we consider diphase micro- and nanocrystalline materials, which were prepared by mixing the two different powders and pressing them together to a pellet. This way, in contrast to the classic dispersed ionic conductors discussed above, the grain size of both ionic conductor and insulator can be varied over several orders of magnitude. For reviews on nanocrystalline materials, see e.g., [39–41].

Very recently, the ionic conductivity of micro- and

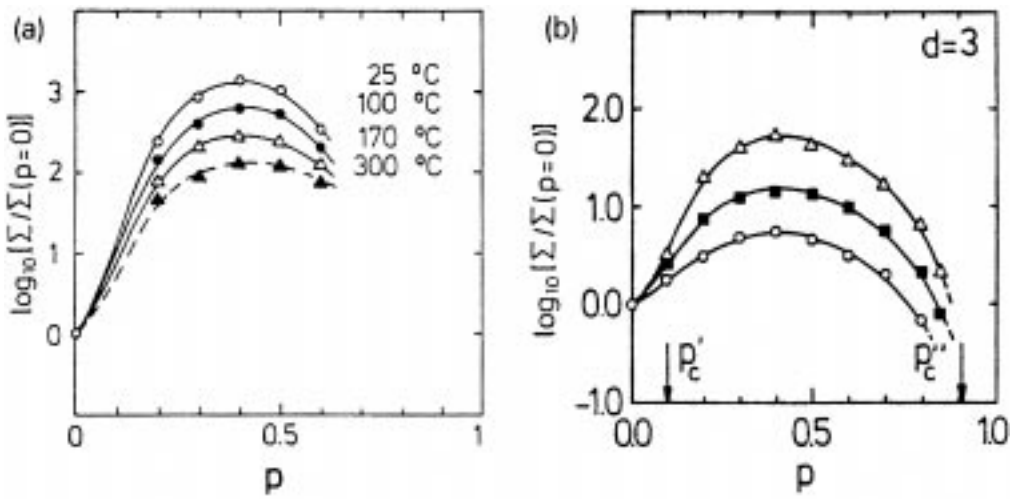

Fig. 8. (a) Normalized conductivity of the LiI-Al_2O_3 system as a function of the mole fraction p of Al_2O_3 at different temperatures (after [32]). (b) Normalized conductivity resulting from Monte Carlo simulations of the three-component percolation model, as a function of p, for $\sigma_A^0/\sigma_B^0 = 10$ (circles), 30 (full squares), and 100 (triangles) (after [30]).

nanocrystalline $(1-x)Li_2O$: xB_2O_3 composites, for different content x of insulator B_2O_3, has been studied by Indris et al. [38]. In the nanocrystalline samples, with an average grain size of about 20 nm, the dc-conductivity increases with increasing content of B_2O_3 up to a maximum at $x \approx 0.5$. Above 0.92, the dc-conductivity vanishes.

In contrast, in the microcrystalline samples (grain size about 10 μm), the dc-conductivity decreases monotonically with x and seems to vanish above $x \approx 0.55$ (see Fig. 9). The activation energy remains almost constant in both cases, $E_{act} \cong 1$ eV, for all x-values.

To explain these surprising experimental observations, Indris et al. assumed that (as for the classical dispersed ionic conductors) (i) B_2O_3 acts as an insulator for the lithium ions, (ii) the mobility of the Li-ions along the diphase boundaries between ionic conductor and B_2O_3 is larger than in the bulk lithium oxide, and (iii) that the thickness λ of this highly conducting interface is independent of the grain size.

For a quantitative treatment one has to note that the insulator content x is related to the volume fraction p (considered in percolation theory) by $p = \alpha x/(\alpha x - x + 1)$, where $\alpha = V_{mol}(B_2O_3)/V_{mol}(Li_2O) \approx 1.9065$ is the ratio between the mole volumes. Accordingly, the experimental results suggest the existence of two different percolation thresholds for the conduction paths, $p_c \approx 0.7$ for the microcrystalline samples and $p_c \approx 0.96$ for nanocrystalline ones, above which the dc-conductivity of the composite vanishes.

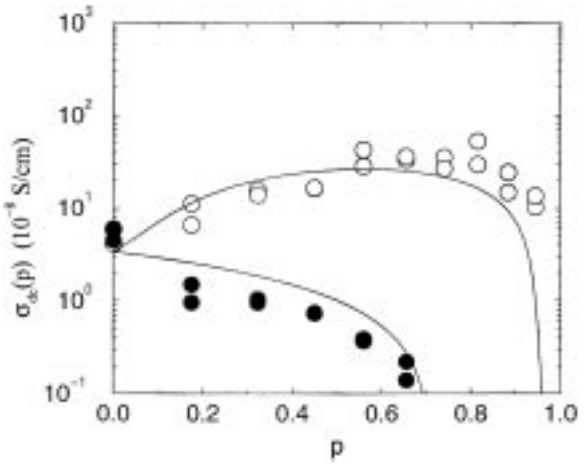

Fig. 9. Plot of the dc-conductivities of the micro- and nanocrystalline composites vs insulator volume fraction p at $T = 433$ K. The conductivity of the nanocrystalline samples (open circles) shows an enhancement up to a maximum at $p \approx 0.7$ ($x \approx 0.5$), while the conductivity of the microcrystalline composites (full circles) decreases monotonically. The lines show the dc-conductivities obtained from the continuum percolation model discussed in the text (after [38]).

These different thresholds can be understood by simple geometrical arguments. In the case of microcrystalline samples, the highly conducting region at the interface between B_2O_3 and Li_2O grains does not play a role since its width is negligible compared to the grain sizes, and conducting paths can open up only when two Li_2O grains get in direct contact to each other. Qualitatively, we can expect a percolating conducting path when the Li_2O concentration gets larger than 0.3 (i.e., $p = 0.7$), which is between the percolation threshold of spheres in a three dimensional continuum percolation model and the percolation threshold of sites in the simple cubic lattice.

In the case of nanocrystalline samples, however, the width of the highly conducting interface becomes comparable to the grain sizes. In this case, the highly conducting region can act as a bridge between two Li_2O grains not in direct contact to each other, opening up additional paths for Li ions. A percolating conducting path can be disrupted only at much higher concentrations of B_2O_3 than for micrometer sized grains. Again, the value suggested by the experiment is in the expected regime.

To describe the actual dependence of the dc conductivity of $Li_2O{:}B_2O_3$ composites, $\sigma_{dc}(p)$, on the insulator concentration p, Indris et al. employed a continuum percolation model similar to that studied earlier for dispersed ionic conductors [35]. In this model, the size of dispersed particles is considered explicitly and the conductivity is estimated by means of the effective medium approximation (EMA), yielding an analytical expression for $\sigma_{dc}(p)$. Denoting by $P_0(p)$, $P_A(p)$ and $P_B(p)$, the concentrations of the insulator, the highly conducting diphase boundaries and the ionic conductor, respectively, $\sigma_{dc}(p)$ is given within EMA by,

$$\sigma_{dc}(p) = \sigma_B^0 \frac{1}{z-2}\left[-A + (A^2 + 2\tau[z-2-zP_0])^{1/2}\right] \tag{22}$$

where $A = \tau(1 - zP_A/2) + (1 - zP_B/2)$, z is a parameter determining the percolation threshold p_c at which $\sigma_{dc} = 0$, and $\tau = \sigma_A^0/\sigma_B^0$ is (as before) the

enhancement factor, defined as the ratio between the conductivities of the highly conducting interface and of pure Li_2O, respectively. For details of the treatment, we refer to [35,38]. The concentrations of the three components are given by $P_0(p) = p$, $P_B(p) = (1-p)^{\eta^3}$ and $P_A(p) = 1 - p - P_B(p)$, with

$$\eta = \frac{R + \lambda}{R} \tag{23}$$

where R is the radius of the particles ($R \cong 10\,\text{nm}$ for the nanoparticles and $R \cong 5\mu\text{m}$ for the microparticles) and λ between 1 and 2 nm.

According to Eq. (22), the percolation threshold for the disruption of conducting paths, p_c, is given by $p_c = (z-2)/z$. Thus, from our previous discussion, we expect that for nanocrystalline samples, $p_c \approx 0.96$, obtaining $z_{nano} = 59$, while in the microcrystalline case $p_c \approx 0.7$ and $z_{poly} = 7$. The remaining parameters, except the interface conductivity σ_A^0 can be easily estimated from the measurements. The theoretical results, obtained for a reasonable fit of σ_A^0, are displayed in Fig. 9 as straight thin lines. The agreement is quantitatively good in view of the simplicity of the model employed.

Both nanocrystalline and microcrystalline materials have been described within the same model. The striking difference between both is the parameter η; $\eta - 1$ describes the thickness of the interface in relation to the grain size. For η close to one, the blocking effect of the large insulating grains dominates, and the dc conductivity decreases monotonically, while for smaller grain sizes a similar behavior as in the classic dispersed ionic conductors occurs.

We like to thank our coworkers in this field, Richard Blender, Paul Heitjans, Silvio Indris, Philipp Maass, H. Eduardo Roman and M. Yussouff, as well as Klaus Funke and Joachim Maier, for many stimulating discussions.

References

1. A. Bunde and S. Havlin (eds.), *Fractals and Disordered Systems* 2nd ed. (Springer Verlag, Heidelberg, 1996).
2. D. Stauffer and A. Aharony, *Introduction to Percolation Theory* (Taylor & Francis, London, 1992).
3. M. Sahimi, *Application of Percolation Theory* (Taylor & Francis, London, 1994).
4. U. Lauer and J. Maier, *Ber. Bunsenges. Phys. Chem.*, **96**, 111 (1992).
5. Z. Ball, H.M. Phillips, D.L. Callahan, and R. Sauerbrey, *Phys. Rev. Lett.*, **73**, 2099 (1994).
6. R.F. Voss, R.B. Laibowitz, and E.I. Allessandrini, *Phys. Rev. Letters*, **49**, 1441 (1982).
7. S. Alexander and R.L. Orbach, *J. Phys. Lett. (Paris)*, **43**, L625 (1982).
8. S. Feng, B.I. Halperin, and P. Sen, *Phys. Rev. B*, **35**, 197 (1987).
9. A.M. Dykne, *Zh. Eksper. Theor. Fiz.*, **59**, 111 (1970).
10. J.P. Straley, *J. Phys. C*, **9**, 783 (1976); *Phys. Rev. B*, **15**, 5733 (1977).
11. A.L. Efros and B.I. Shklovskii, *Phys. Stat. Sol. B*, **76**, 475 (1976).
12. D. Stroud and D.J. Bergmann, *Phys. Rev. B*, **25**, 2061 (1982).
13. J.P. Clerc, G. Giraud, J.M. Langier, and J.M. Luck, *Advances in Physics*, **39**, 191 (1990).
14. S. Havlin and D. Ben-Avraham, *Advances in Physics*, **36**, 695 (1987).
15. B. Derrida and J. Vannimenus, *J. Phys. A: Math. Gen.*, **15**, L557 (1982).
16. S. Kirkpatrick, *Rev. Mod. Phys.*, **45**, 574 (1973).
17. H. Boettger and V.V. Bryksin, *Hopping Conduction in Solids* (VCH, Weinheim, 1985), ch. 3.
18. C. Pecharromin and J.E. Iglesias, *Phys. Rev. B*, **49**, 7137 (1994).
19. E.J. Garboczi, K.A. Snyder, J.F. Douglas, and M.F. Thorpe, *Phys. Rev. E*, **52**, 819 (1995).
20. T.K. Ballabh, T.R. Middya, and A.N. Basu, *J. Phys. D: Appl. Phys.*, **21**, 567 (1988); *ibid.*, **22**, 1434 (1989).
21. K. Mussawisade, T. Wichmann, and K.W. Kehr, *J. Phys.: Condens. Matter*, **9**, 1181 (1997).
22. P. Maass, B. Rinn, and W. Schirmacher, *Phil. Mag. B*, **79**, 1915 (1999).
23. R.B. Stinchcombe and B.P. Watson, *J. Phys. C*, **9**, 3221 (1976).
24. J. Bernasconi, *Phys. Rev. B*, **18**, 2185 (1978).
25. D.J. Frank and C.J. Lobb, *Phys. Rev.*, **37**, 302 (1988).
26. C. C. Liang, *J. Electrochem. Soc.*, **120**, 1289 (1973).
27. For a review see A. K. Shukla and V. Sharma, in: *Solid State Ionics: Materials and Applications* eds. B.V.R. Chowdari, S. Chandra, S. Singh and P.C. Srivastava (World Scientific, Singapore, 1992) p. 91.
28. J. Maier in: *Superionic Solids and Electrolytes* ed. by A.L. Laskar and S. Chandra (Academic Press, New York, 1989) p. 137.
29. A. Bunde, W. Dieterich, and E. Roman, *Phys. Rev. Lett.*, **55**, 5 (1985).
30. H.E. Roman, A. Bunde, and W. Dieterich, *Phys. Rev. B*, **64**, 35 (1986).
31. R. Blender and W. Dieterich, *J. Phys. C*, **20**, 6113 (1987).
32. F.W. Poulsen, N. Hessel Andersen, B. Kinde, and J. Schoonman, *Solid State Ionics*, **9/10**, 119 (1983).
33. Chen Li-Quang et al., *Acta Phys. Sin.*, **34**, 1027 (1984).
34. H.E. Roman and M. Yussouff, *Phys. Rev. B*, **36**, 7285 (1987).
35. H.E. Roman, *J. Phys.: Condens Matter*, **2**, 3909 (1990).
36. A.J. Bhattacharya, T. Dutta, S. Roy, S. Tarafdar, and T.R. Middya, in: *Materials Science Forum* 223–224, eds. D.K. Chaturvedi and G.E. Murch (Transtec Publications, Switzerland, 1996) p. 279.
37. G.M. Zhang, *Phys. Rev. B*, **53**, 6256 (1996).
38. S. Indris, P. Heitjans, H.E. Roman, and A. Bunde, *Phys. Rev. Lett.*, **84**, 2889 (2000).
39. H. Gleiter, *Progress in Material Science*, **33**, 223 (1989).
40. R.W. Siegel, *Encyclopedia of Applied Physics*, **11**, 173 (1994).
41. J. Maier, *Prog. Solid St. Chem.*, **23**, 171 (1995).